Damage Localization Based on MUSIC Beamforming Algorithm Under Variable Temperature Conditions

XIAOZHEN ZHANG, JINSONG YANG and TIANTIAN WANG

ABSTRACT

Environmental temperature variations pose significant challenges in Lamb wave-based structural health monitoring by introducing amplitude and phase distortions that can mask damage-related signal features. This paper presents a novel damage imaging and localization method integrating an improved Multiple Signal Classification (MUSIC) algorithm with beamforming techniques to address these challenges. An array signal propagation model has been developed to explicitly account for temperature-induced effects on wave propagation characteristics, while an enhanced MUSIC algorithm incorporating amplitude-phase error compensation through cost function optimization has been formulated to mitigate signal distortions. The method further employs beamforming-based spatial filtering to improve imaging resolution under varying temperature conditions. The effectiveness of the proposed method has been validated through extensive experimental studies conducted on aluminum plates with square hole damages under temperatures ranging from -40°C to 80°C. Results demonstrate that the method achieves consistent damage localization accuracy with relative errors maintained below 5.69% across all temperature conditions, while successfully preserving imaging resolution and boundary definition. The method's robust performance and computational efficiency make it particularly suitable for practical structural health monitoring applications where temperature variations are inevitable.

1. INTRODUCTION

Structural health monitoring (SHM) has attracted significant attention in recent decades due to its crucial role in ensuring operational safety and maintenance efficiency[1][2][3]. Lamb wave-based methods have emerged as particularly promising approaches due to their high sensitivity to structural damage and capability for large-area monitoring[4][5][6][7]. Ultrasonic wavefield imaging techniques have enabled direct visualization of wave propagation across structural surfaces, facilitating damage inference through wavefield pattern variations[8][9]. However, environmental variations, especially temperature fluctuations, significantly challenge these methods' reliability, particularly in aerospace and high-speed rail applications[14][15].

To address damage detection challenges under complex environmental conditions, researchers have developed various signal processing techniques based on piezoelectric sensor arrays. Wang et al.[16] developed a phased array ultrasonic method for composite plate damage localization. Wang Zhiling et al.[17] proposed an ultrasonic phased array-based structural multi-damage monitoring method. Yang et al.[18] integrated the Multiple Signal Classification (MUSIC) algorithm with electrodynamics theory for impact source localization. Su Yongzhen et al.[19] combined the MUSIC

Corresponding author: Jinsong Yang, E-mail address: yangjs@csu.edu.cn, School of Transportation Engineering, Central South University, No. 22 Shaoshan South Road, Tianxin District, Changsha City, Hunan Province, China, Postal Code: 410075.

algorithm with wavelet transform to enhance composite structure impact localization. Zhong et al.[20] proposed an improved method combining optimized Ensemble Empirical Mode Decomposition (EEMD) with two-dimensional MUSIC algorithm. Zuo et al.[21] developed a 2D-MUSIC algorithm for plate structure damage identification based on wave propagation models. While promising in laboratory environments, these methods' performance under varying temperature conditions requires further investigation.

Multiple researchers have confirmed that environmental variations, particularly temperature fluctuations, can mask damage-related signal changes. Radecki et al.[22] investigated temperature effects on Lamb wave characteristics, proposing a clustering algorithm for damage assessment. Sikdar et al.[23] studied delamination influence on Lamb wave propagation under varying temperatures. Marzania et al.[24] proposed a numerical method to predict temperature effects on guided waves from -40°C to +60°C. Bao et al.[25] addressed structural anisotropy by proposing an anisotropy-compensated MUSIC method. Zhang et al.[26] examined temperature effects on wave propagation signals, proposing an improved MUSIC method with phase correction. However, these methods generally require extensive experimental correction of sensor phase errors and focus primarily on phase compensation while neglecting amplitude variations, limiting their practical applicability.

2. METHODOLOGY DEVELOPMENT

2.1 MUSIC AND BEAMFORMING ALGORITHM

The MUSIC algorithm performs DOA estimation by separating signal and noise subspaces through eigen decomposition of the array signal covariance matrix. This estimation leverages the orthogonality between signal steering vectors and the noise subspace to construct a spatial scanning spectrum. The incident angle θ represents the angle between each source direction and the normal vector of the first array element. The received signal matrix X(t) is formulated according to Eq (1).

$$\mathbf{X}(t) = \mathbf{A}(\theta)\mathbf{S}(t) + \mathbf{N}(t) \tag{1}$$

where $A(\theta)$, $A(t)$, and $N(t)$ are expressed as:

$$\mathbf{A}(\theta) = \left[a(\theta_1), a(\theta_2), \cdots, a(\theta_M)\right]^{\mathrm{T}} = \begin{bmatrix} 1 & \cdots & 1 \\ \mathrm{e}^{-\mathrm{j}\sin\theta_1} & \cdots & \mathrm{e}^{-\mathrm{j}\sin\theta_M} \\ \vdots & & \vdots \\ \mathrm{e}^{-\mathrm{j}(M-1)\sin\theta_1} & \cdots & \mathrm{e}^{-\mathrm{j}(M-1)\sin\theta_M} \end{bmatrix}^{\mathrm{T}} \tag{2}$$

$$\mathbf{S}(t) = \left[S_1(t), S_2(t), \cdots, S_M(t)\right]^T \tag{3}$$

$$\mathbf{N}(t) = \left[n_1(t), n_2(t), \cdots, n_N(t)\right] \tag{4}$$

where $A(\theta)$ represents the steering matrix of the linear array, $S(t)$ denotes the signal matrix of M far-field sources with incident angles θ relative to the normal vector of the first array element, and $N(t)$ is the noise matrix.

The cross-correlation matrix of the received signals is defined as $\mathbf{R}_x = \mathrm{E}\left[XX^{\mathrm{H}}\right]$, where the superscript H denotes the Hermitian transpose of the matrix. Assuming that the noise is uncorrelated, zero-mean additive Gaussian white noise, substitution of Eq (5) yields:

$$\mathbf{R}_x = \mathrm{E}\left[(\mathbf{A}(\theta)\mathbf{S}(t) + \mathbf{N}(t))(\mathbf{A}(\theta)\mathbf{S}(t) + \mathbf{N}(t))^{\mathrm{H}}\right] = \mathbf{A}\mathbf{E}\left[SS^{\mathrm{H}}\right]\mathbf{A}^{\mathrm{H}} + \mathrm{E}\left[NN^{\mathrm{H}}\right] = \mathbf{A}\mathbf{R}_S\mathbf{A}^{\mathrm{H}} + \mathbf{R}_N \tag{5}$$

Where $R_S = \mathbf{E}\left[SS^{\mathrm{H}}\right]$ represents the signal correlation matrix, $R_N = \sigma^2 I$ denotes the noise correlation matrix, σ^2 is the variance of the noise signal, and I represents the $M \times M$

identity matrix. Let $\{\lambda_1, \lambda_2, \cdots \lambda_N\}$ be the eigenvalues of the covariance matrix R with corresponding eigenvectors $\{q_1, q_2, \cdots q_N\}$. When multiple sources are uncorrelated and the number of sources M＜N, R is positive semi-definite, containing M larger eigenvalues and (N-M) smaller eigenvalues equal to σ^2. Arranging the eigenvalues of matrix $\mathbf{R}_x$ in descending order yields $\lambda_1 > \lambda_2 > \cdots > \lambda_M \cdots > \lambda_N$, where the M larger eigenvalues correspond to the signal subspace, and the remaining (N-M) smaller eigenvalues correspond to the noise subspace. The eigenvectors associated with the signal eigenvalues and noise eigenvalues are designated as signal eigenvectors and noise eigenvectors, respectively.

According to the definition of eigenvalues and eigenvectors:

$$\mathbf{R}_x q_i = \lambda_i q_i \tag{6}$$

Multiplying both sides of Equation (16) by q_k yields:

$$\mathbf{R}_x q_k = \left(\mathbf{A}\mathbf{R}_S \mathbf{A}^{\mathrm{H}} + \sigma^2 \mathbf{I}\right) q_k = \mathbf{A}\mathbf{R}_S \mathbf{A}^{\mathrm{H}} q_k + \sigma^2 q_k \tag{7}$$

$$\mathbf{A}\mathbf{R}_S \mathbf{A}^{\mathrm{H}} q_k = 0 \tag{8}$$

$$\begin{aligned} &\mathbf{R}_S^{-1} \left(\mathbf{A}^{\mathrm{H}} \mathbf{A}\right)^{-1} \mathbf{A}^{\mathrm{H}} \mathbf{A}\mathbf{R}_S \mathbf{A}^{\mathrm{H}} q_k = 0 \\ &\mathbf{A}^{\mathrm{H}} q_k = 0 \end{aligned} \tag{9}$$

$$\mathbf{R}_x q_k = \left(\mathbf{A}\mathbf{R}_S \mathbf{A}^{\mathrm{H}} + \sigma^2 \mathbf{I}\right) q_k = \mathbf{A}\mathbf{R}_S \mathbf{A}^{\mathrm{H}} q_k + \sigma^2 q_k \tag{10}$$

Eq(10) establishes orthogonality between noise eigenvectors and steering vectors. This property enables DOA estimation via spatial spectrum generation, with EN derived from array signal cross-correlation matrix.

$$P(\theta) = \frac{1}{\mathbf{A}^{\mathrm{H}}(\theta) \mathbf{E}_N \mathbf{E}_N^{\mathrm{H}} \mathbf{A}(\theta)} \tag{11}$$

Spatial filtering processes linear array signals through delay adjustment, weighting, and summation to achieve directional gain control. Traditional beamforming employs phase-shift or time-delay methods to enhance desired signals while suppressing others, effectively extracting low-amplitude damage signals from noise. This study utilizes the CBF algorithm, based on time-delay-weight-sum methodology, for spatial filtering of damage signals, as expressed in Equation (12).

$$y_{\theta_0}(t) = \sum_{n=1}^{N} w_n x_n(t) = \sum_{n=1}^{N} \mathrm{e}^{-\mathrm{j}2\pi f^{(n-1)d\sin\theta_0}} x_n(t) \tag{12}$$

2.2 ARRAY LAMB WAVE MODELING UNDER VARIABLE TEMPERATURE ENVIRONMENT

Temperature variations significantly impact Lamb wave propagation, introducing amplitude and phase uncertainties in received signals. A modified array signal model incorporating temperature-dependent parameters is necessary, with reference point O as array center and symmetrically distributed sensors. Temperature affects wave velocity and material properties, causing variable amplitude attenuation and phase shifts across elements. For a uniform linear array with 2M+1 elements under temperature variations, the q-th element's received signal is modeled as:

$$x_q(t) = \frac{r}{r_q} s(t) \mathrm{e}^{-\mathrm{j}\omega_0 \tau_q} + n_q(t) \tag{13}$$

where q = -M, ,0, ,M, r and rq represent the distances from the damage source to the reference point $0\#$ and the $q\#$ array element, respectively. $s(t)$ denotes the damage

source signal, and $n_q(t)$ represents the noise signal. The path difference τ_q between the damage source arrivals at the $0\#$ and $q\#$ sensor elements can be expressed as:

$$\tau_q = \frac{(-d\sin\theta)}{c}(q-1) + \left(-\frac{d^2}{cr}\cos^2\theta\right)(q-1)^2 + O\left(\frac{d^2}{r^2}\right) \tag{14}$$

where r and d represent the amplitude and phase delay associated with the q-th array element sensor due to temperature variations.

Let $a_q(r,\theta)$ represent the array steering vector of the near-field damage signal, which can be expressed as:

$$a_q(r,\theta) = \frac{r}{r}\exp\left(-\mathrm{j}\omega_0\tau_q\right) \tag{15}$$

The modified observation data from the q-th array element can be expressed as:

$$x(t) = \alpha_q s\left(t-\tau_q-\psi_q\right) + n_q(t) \tag{16}$$

Let Γ_q denote the amplitude-phase error of the $\Gamma-th$ array element, which can be represented as:

$$\Gamma_q = \alpha_q \exp\left(-\mathrm{j}w_0\psi_q\right), q = -M,\cdots,M \tag{17}$$

The array sensor error matrix is thus derived as:

$$\mathbf{\Gamma}(r,\theta) = \mathrm{diag}\left\{\mathbf{\Gamma}_{-M},\cdots,\mathbf{\Gamma}_M\right\} \tag{18}$$

By incorporating the error matrix, the array steering vector for near-field damage signals can be expressed as:

$$\widetilde{\mathbf{A}}(r,\theta) = \mathbf{\Gamma}(r,\theta)\mathbf{A}(r,\theta) \tag{19}$$

For a uniform linear array, the observed input array signal vector is given by:

$$\mathbf{X}(t) = \widetilde{\mathbf{A}}(r,\theta)\mathbf{s}(t) + \mathbf{N}(t) \tag{20}$$

where:

$$\begin{aligned}
&\mathbf{X}(t) = \left[x_{-M}(t),\cdots,x_0(t),\cdots,x_M(t)\right]^{\mathrm{T}} \\
&\widetilde{\mathbf{A}}(r,\theta) = \left[\tilde{a}_{-M}(r,\theta),\cdots,\tilde{a}_0(r,\theta),\cdots,\tilde{a}_M(r,\theta)\right]^{\mathrm{T}} \\
&\mathbf{N}(t) = \left[\mathbf{n}_{-M}(t),\cdots,\mathbf{n}_0(t),\cdots,\mathbf{n}_M(t)\right]^{\mathrm{T}}
\end{aligned} \tag{21}$$

The covariance matrix of the sensor array observation signal vector under variable temperature field conditions is:

$$\mathbf{R}_x = E\left[\mathbf{X}\mathbf{X}^{\mathrm{H}}\right] = \mathbf{\Gamma}\mathbf{A}\mathbf{R}_{\mathrm{s}}\mathbf{A}^{\mathrm{H}}\mathbf{\Gamma}^{\mathrm{H}} + \delta^2\mathbf{I} \tag{22}$$

where $\mathbf{R}_{\mathrm{s}}$ represents the signal subspace covariance matrix, δ^2 denotes white noise, and H indicates the conjugate transpose. The eigenvalue decomposition of $\mathbf{R}_x$ yields：

$$\mathbf{R}_x = \mathbf{U}_{\mathrm{S}}\sum_{\mathrm{s}}\mathbf{U}_{\mathrm{S}}^{\mathrm{H}} + \mathbf{U}_{\mathrm{N}}\sum_{\mathrm{N}}\mathbf{U}_{\mathrm{N}}{}^{\mathrm{H}} \tag{23}$$

where $\mathbf{U}_{\mathrm{S}}$ represents the signal subspace corresponding to the largest eigenvalue $\sum_s$, and $\mathbf{U}_{\mathrm{N}}$ represents the noise subspace corresponding to the smallest eigenvalue $\sum_N$.

To characterize the orthogonal properties, the spatial spectrum of the sensor array under variable temperature field conditions can be calculated through:

$$P = \mathbf{A}(r,\theta)^{\mathrm{H}}\mathbf{\Gamma}^{\mathrm{H}}U_{\mathrm{N}}U_{\mathrm{N}}^{\mathrm{H}}\mathbf{\Gamma}\mathbf{A}(r,\theta) = \left\|U_{\mathrm{N}}^{\mathrm{H}}\mathbf{\Gamma}\widetilde{\mathbf{A}}(r,\theta)\right\|^2 \tag{24}$$

A cost function must be developed to jointly estimate damage location parameters and amplitude-phase errors under temperature variations. The MUSIC algorithm's core

principle—orthogonality between true damage location steering vector and noise subspace—is compromised by temperature-induced uncertainties. We propose a cost function J that quantifies the temperature-compensated steering vector's projection onto the noise subspace. Minimizing this function enables simultaneous optimization of damage location parameters and amplitude-phase error matrix, improving localization accuracy under variable temperature conditions.

$$J(r,\theta,\Gamma)=\boldsymbol{\gamma}^{\mathrm{H}}\left\|\mathbf{A}(r,\theta)^{\mathrm{H}}U_{\mathrm{N}}U_{\mathrm{N}}^{\mathrm{H}}\mathbf{A}(r,\theta)\right\|\gamma \tag{25}$$

Where: $\boldsymbol{\gamma}=\left[\boldsymbol{\Gamma}_{-M},\cdots,\boldsymbol{\Gamma}_{M}\right]^{\mathrm{T}}$.

3.THE DAMAGE IMAGING EXPERIMENTS

3.1 EXPERIMENT SETUP

Fig. 1 illustrates the experimental setup, consisting of a sensing/data acquisition system and environmental enclosure. The SHM system operates at 60 MHz sampling frequency with 12-bit resolution. Temperature control is maintained by an environment box with 0.1°C accuracy. PZT and structure properties are detailed in Tables 1. Testing spans -40°C to 80°C. Collection occurs only when target temperatures are reached. Lamb wave excitation uses 160 kHz center frequency with 10 MHz sampling.

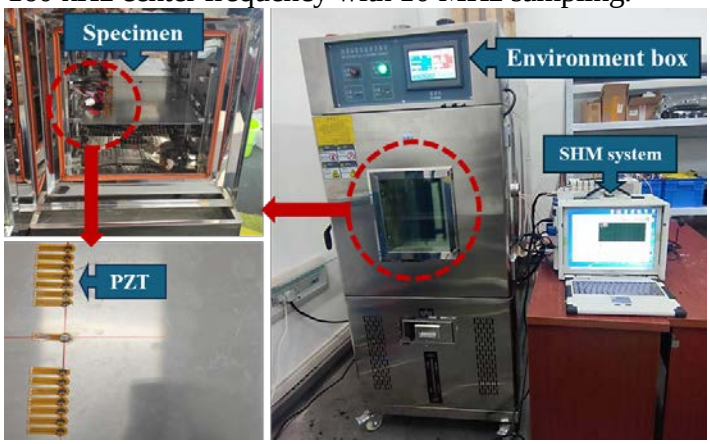

Fig. 1 Overall diagram of experimental equipment

The test specimen is made of 6061aluminum. The mechanical properties are listed in Table The geometry of the specimen is 200mm*200 mm*2 mm. The sensor layout is shown in Fig. 2.

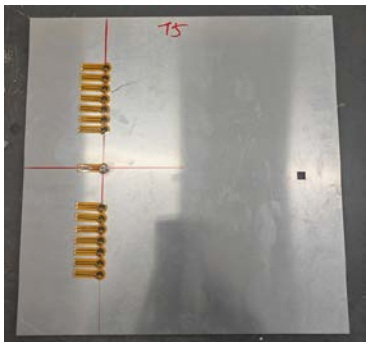

Fig. 2 PZT sensor layout

Table 1. Model and parameters of the structure

Material: Al6061	Normal temperature
Young's modulus	68.9
Poisson's ratio	0.33
Density	2750 kg/m^3

Geometrical dimensions	200 mm×200 mm×2 mm

4. Data analysis

Fig.3 displays damage localization imaging results from -40°C to 80°C. Imaging quality and resolution remain consistent across temperatures. At -40°C, slight blurring occurs due to enhanced signal attenuation. Optimal performance was achieved at 20°C with distinct damage boundaries. Despite modest degradation at 80°C, localization accuracy remains uncompromised, validating the method's robustness across thermal conditions.

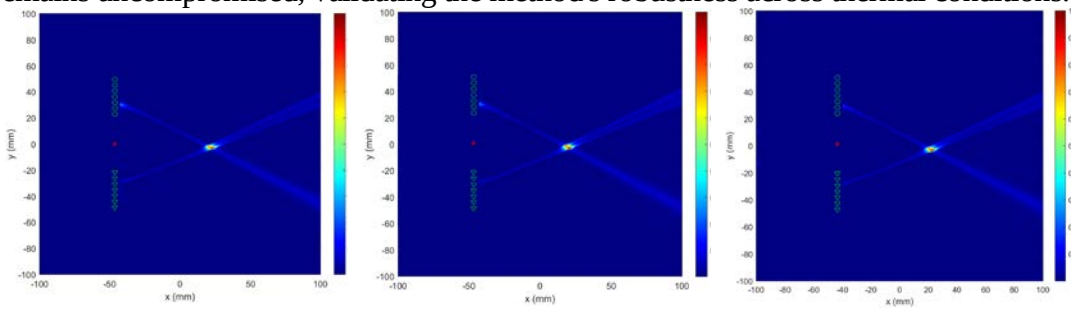

(a)-40℃ (c)20℃ (c)80℃

Fig. 3 Damage localization results under different temperatures

To evaluate the positioning accuracy, relative error is used as the evaluation index. Assuming the actual coordinates of the damage location are (x_0, y_0), the coordinates obtained from localization are (x_1, y_1). Calculate the Euclidean distance between the actual point and the positioning point:

$$d_{error} = \sqrt{(x_0 - x_1)^2 + (y_0 - y_1)^2} \tag{26}$$

Calculate the distance from the actual damage point to the coordinate origin:

$$d_{actual} = \sqrt{x_0^2 + y_0^2} \tag{27}$$

The relative error can be expressed as:

$$\varepsilon = \frac{d_{error}}{d_{actual}} \times 100\% \tag{28}$$

Table 2 Damage localization errors under different temperatures

Temperatures	-40℃	20℃	80℃
True position	(25, 5)	(25, 5)	(25, 5)
Detecting location	（23.5,3.9）	(25.8,5.5)	(23.7,6.4)
Relative error	7.30%	3.70%	7.49%

Table 2 quantifies localization accuracy across temperatures. Analysis reveals consistent performance throughout the tested range, with optimal precision at 20°C (3.70% relative error). Performance slightly deteriorates at extremes, with maximum deviations at -40°C (7.30%) and 80°C (7.49%), yet remains within acceptable parameters. These results validate the amplitude-phase error compensation mechanism's effectiveness in mitigating temperature-induced perturbations. The consistently low relative errors confirm the integrated MUSIC-beamforming methodology's robustness in maintaining precise damage localization despite significant thermal fluctuations. Experimental results demonstrate successful temperature compensation, stable spatial resolution, and reliable accuracy across the -40°C to 80°C operational range, establishing the method's viability for structural health monitoring in variable temperature environments.

5. CONCLUSION

A novel Lamb wave-based damage imaging methodology for variable temperature conditions has been proposed and validated, integrating improved MUSIC algorithm with beamforming techniques. Key conclusions include:

(1) The developed MUSIC algorithm with amplitude-phase error compensation effectively addresses temperature-induced signal variations through cost function optimization. Experimental validation confirms consistent localization accuracy from -40°C to 80°C with acceptable positioning errors.

(2) Beamforming integration enhances spatial filtering and imaging resolution, successfully suppressing environmental noise while preserving damage-related signal features, thereby improving detection reliability under variable temperatures.

(3) Experimental validation on aluminum plates demonstrates robust performance with relative positioning errors below 7.5% across all temperature conditions, confirming practical applicability in real-world monitoring scenarios where temperature variations occur.

REFERENCES

1. Sunquan Yu ,Kai Luo, Chengguang Fan,et al. Advancing spacecraft safety and longevity: A review of guided waves-based structural health monitoring[J] .Reliability Engineering and System Safety,2025, 254:110586.
2. Chen J , Meng Y , Xu Y .A multi-layer ML model evolutionary paradigm for high-accuracy individual aircraft SHM[J].Aerospace science and technology, 2024, 144(Jan.):108824.1-108824.15.DOI:10.1016/j.ast.2023.108824.
3. Yuan S , Jing H , Zhang W J .A whole service time SHM damage quantification model hierarchical evolution mechanism[J].Mechanical Systems & Signal Processing, 2024, 209(Mar.):111064.1-111064.19.DOI:10.1016/j.ymssp.2023.111064.
4. Luo K , Zhu J , Li Z ,et al.Ultrasonic Lamb Wave Damage Detection of CFRP Composites Using the Bayesian Neural Network[J].Journal of Nondestructive Evaluation, 2024, 43(2).DOI:10.1007/s10921-024-01054-z.
5. KimBeomjin, Ugli M A K , Kimyoung H ,et al.Tomography of wall-thinning defect in plate structure based on guided wave signal acquisition by numerical simulations[J].Journal of Visualization, 2024.DOI:10.1007/s12650-024-00977-z.
6. Yang Z , Zhang J , Xu H ,et al.Phased Array System for Damage Detection in Plate-Like Structures Based on Single Lamb Wave Mode Extraction[J].Journal of Aerospace Engineering, 2023.DOI:10.1061/jaeeez.aseng-4543.
7. Li X , Liu L , Xu H ,et al.Lamb wave phased array imaging based on phase-amplitude compounding algorithm[J].Mechanical Systems and Signal Processing, 2023, 205.DOI:10.1016/j.ymssp.2023.110882.
8. He Y , Wang K , Xu L ,et al.Laser ultrasonic imaging of submillimeter defect in a thick waveguide using entropy-polarized bilateral filtering and minimum variance beamforming[J].Mechanical Systems and Signal Processing, 2023.DOI:10.1016/j.ymssp.2022.109863.
9. Chen W , Wang B , Chen J ,et al.Development of a High-Frequency Mini-Convex Array Probe for Intraluminal Ultrasonic Imaging Applications[J].IEEE sensors journal, 2024(11):24.DOI:10.1109/JSEN.2024.3392915.
10. Bin Z , Zhuyun C , Gang X J .An intelligent ultrasonic guided wave deep imaging detection method considering the propagation characteristics of each direction[J].Measurement Science & Technology, 2023, 34(1):014006-1-014006-13.
11. Yn L S , Romli F I , Mazlan N ,et al.High-Resolution Wavenumber Bandpass Filtering of Guided Ultrasonic Wavefield for the Visualization of Subtle Structural Flaws[J].Aerospace (MDPI Publishing), 2024, 11(7).DOI:10.3390/aerospace11070524.
12. Luo K , Liu Y , Yang C Z .Rapid damage reconstruction imaging of composite plates using

non-contact air-coupled Lamb waves[J].NDT & E International: Independent Nondestructive Testing and Evaluation, 2024, 143(Apr.):103047.1-103047.13.
13. Zhu W , Xiang Y , Zhang H ,et al.Super-resolution ultrasonic Lamb wave imaging based on sign coherence factor and total focusing method[J].Mechanical Systems and Signal Processing, 2023.DOI:10.1016/j.ymssp.2023.110121.
14. Zhang X , Wang T , Yang J ,et al.Adaptive crack damage identification based on multi-scale sample entropy under variable temperature environment[J].Mechanical Systems & Signal Processing, 2024(Feb.):208.DOI:10.1016/j.ymssp.2023.111061.
15. Zhang X , Wang T , Yang J ,et al. Quantitative evaluation of crack damage under a variable temperature environment based on a Gaussian mixture model[J]. Structural Health Monitoring,2022, 22(3):147592172211180.
16. WANG X Y, HE J J, GAO W H, et al. Three-dimensional damage quantification of low velocity impact damage in thin composite plates using phased-array ultrasound[J]. Ultrasonics, 2020, 110: 106264.
17. WANG Z L, YUAN S F, QIU L, et al. Multi-damage monitoring method based on piezoelectric ultrasonic phased array[J]. Journal of Vibration, Measurement & Diagnosis, 2014(5): 796-801..
18. YANG H, LEE Y J, Lee S K. Impact source localization in plate utilizing multiple signal classification[C]//Proceedings of the Institution of Mechanical Engineers Part C-Journal of Mechanical Engineering Science, 2013, 227: 703-713.
19. SU YZ, YUAN S F, WANG Y. Impact localization in composite using multiple signal classification method [J]. Acta Materia Compositae Sinica,2010(3):105-110.
20. ZHONG YT, XANG IW, CHENX.et al. Multiple signal classification-based impact localization in composite structures using optimized ensemble empirical mode decomposition[J]. Appl. Sci, 2018, 8(9): 1447.
21. ZUO H, YANG Z, Xu C, et al Damage identification for plate-like structures using ultrasonic guided wave based on improved MUSIC method[J]. Composite Sucher, 2018, 203:164-171.
22. Radecki R, Staszewski W J, Uhl T. Impact of changing temperature on lamb wave propagation for damage detection[J]. Key Engineering Materials, 2014, 588:140-148.
23. Sikdar S, Fiborek P, Kudela P, et al. Effects of debonding on Lamb wave propagation in a bonded composite structure under variable temperature conditions[J]. Smart Materials &Structures, 2019,28:015021.
24. Francesco Lanza di Scalea, Salvatore Salamone. Temperature effects in ultrasonic lamb wave structural health monitoring systems [J]. Journal of the Acoustical Society of America. 2008.161https://doi.org/10 1121/1.2932071
25. BAO O, YUAN S F, WANG YW, et al. Anisotropy compensated MUSIC algorithm based composite structure damage imaging method[J]. Composite Structure, 2019,214:293-303.
26. ZHANG Z H, ZHONG Y T, XANG JW, et al Phase correction improved multiple signal classification for impact source localization under varying temperature condition[J].Measurement,2020,152107374.